

Original Article

Influence of prior austenite grain size distribution on the microstructure and mechanical properties of a welded micro-alloyed ABS EH36 steel

Ganwarich Pluphrach* and Tri Kharanan

*Department of Mechanical Engineering, Faculty of Engineering,
Srinakharinwirot University, Ongkharak, Nakhon Nayok, 26120 Thailand*

Received: 19 March 2019; Revised: 21 July 2019; Accepted: 6 August 2019

Abstract

Main objective of the study was to investigate the prior austenite grain size distribution on microstructures and mechanical properties of welded micro-alloyed ABS EH36 steel. Shielded metal arc welding (SMAW) is processed using AWS A5.1 E7016, Dia. 2.6 mm welding electrode to prepare the weldments. A relationship between diameter and number of austenite and ferrite grains is analyzed to evaluate the mean austenite and ferrite grain size of the steel using Spektor's model. The large grain size dominates the nucleation of ferrite, where the kinetics information should be related to the large grain and will contribute to meet the increasing low temperature toughness requirement of weld metals for the shipbuilding industry. Effectiveness yield stresses are controlled by applying different mean ferrite grain size according to Hall-Petch model. It is found that all grain size distribution and yield stresses of the three welded zones steel are in good correlation.

Keywords: prior austenite grain size, welded micro-alloyed ABS EH36 steel, linear intersection chords distributions, model

1. Introduction

Micro-alloyed high-strength low-alloy (HSLA) steels are essentially low carbon low-alloy steels that contain small additions (0.001-0.1 wt.%) of alloying elements such as Nb, V, or Ti. These steels exhibit an outstanding combination of high strength, resistance to brittle fracture and good weldability, particularly if the carbon content is kept below ~0.1 wt.%. Several categories of HSLA steels have been developed catering to the needs of specific applications, such as the construction of large ships, oil and gas transmission lines, and offshore oil drilling platforms (Das, Ghosh, Chatterjee, & Ramachandra, 2003; Show, Veerababu, Bala muralikrishnan, & Malakondaiah, 2010; Pluphrach & Yamsai, 2018). Especially, structural offshore steel plate as ABS EH36 has many excellent mechanical properties such as high yield strength, transverse plasticity, fracture toughness, etc., and it

is widely used in the shipbuilding industry both in hull construction and in the superstructure itself. This shipbuilding grade is used in the cabin structures of cruisers and ships, construction structural parts of the ships, barges, marine equipment, ice-breakers, ice-going vessels, bulk cargo vessels, ferries, and yachts in addition to offshore structures and pressure equipment (Chen *et al.*, 2017; Austenite, 2019). Austenite, also known as gamma-phase iron (γ -Fe), is a metallic, non-magnetic allotrope of iron or a solid solution of iron, with an alloying element. It is named after W. Chandler Roberts-Austen (1843–1902) (Austenite, 2019). The prior austenite at room temperature in a structural steel, a typical microstructure of a steel specimen polished surface, after etching in saturated aqueous picric acid solution is finished (Figure 1) (Adrian & Wiencek, 2015; Irshad, 2011). Considering the initial austenite grain size, austenite forms by the nucleation of austenite grains at various locations. Eventually they begin to impinge, and finally the pearlite disappears. At this stage the steel has its initial austenite grain size. From nucleation and growth theory, the number of grains per unit area N_i in a planar cut through a sample is given by (Brooks, 1992)

*Corresponding author
Email address: pganwarich@yahoo.com



Figure 1. Revealing prior-austenite grain boundaries in an as-cast low alloy structural steel (40Cr8) with contents of micro-alloying elements, V, Nb and Ti, heat treated with austenitizing for 30 min in argon atmosphere at temperature in the range of 840-1,200 °C and quenching in water.

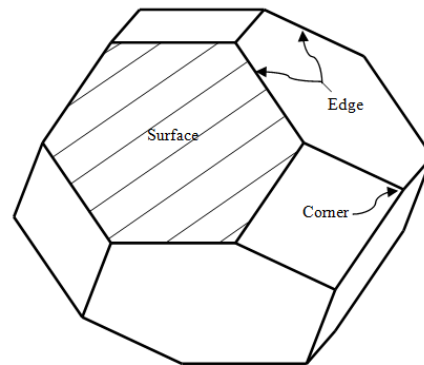
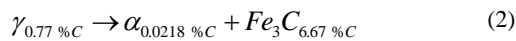


Figure 2. Related three ferrite nucleation sites with the prior austenite grain.

$$N_i = 1.01 (N/G)^{0.5} \tag{1}$$

where N is the nucleation rate and G is the growth rate. From the N_i the grain size can be obtained. Figure 2 shows about the estimation of ferrite grain size formed in this research material, nucleation site is supposed that to occur on four types, i.e. homogeneous sites within the austenite grain, edges, corners and surfaces. At the prior austenite grain surface (Figure 2) (Kazeminezhad & Taheri, 2004), the grain size of ferrite is defined with those ferrite nucleations number till the surface accomplishment with occupied ferrite grains. For the reason, ferrite grain size is free from austenite matrix and is nucleated every growth rates of temperature variation during continuous cooling transformation (Figure 3) (Kazeminezhad & Taheri, 2004) and the eutectoid reaction considered, when austenite temperature cools to 727 °C, the reaction begin as the equation below (Askeland, 1996).



In this micro-alloyed ABS EH36 research steel, one of the important factors influencing various properties is the grain size of austenite. Normally, austenite grain size is roughly evaluated and it is reported only as the mean value. For evaluation the grain size exactly, it is essential to consider the grain size distribution. The grain size distributions are dissimilar shapes depend on the number of dimensions measured (Pluphrach, 2005). Spektor’s method, Spektor considers the penetration of a polydispersed system of spheres by a straight line, or secant (Figure 4) (DeHoff & Rhines, 1968). First, it is assumed that there are many spheres of diameter d_j , the centers of which are distributed in space with statistical uniformity. The distance from the center of the sphere to the intersecting chord is

$$x(i, j) = \sqrt{\left(\frac{d_j}{2}\right)^2 - \left(\frac{l_i}{2}\right)^2} \tag{3}$$

where l_i is the length of the chord. The number of chords per unit length of the secant having lengths between l_i and d_j is calculated next. These chords must belong to only those

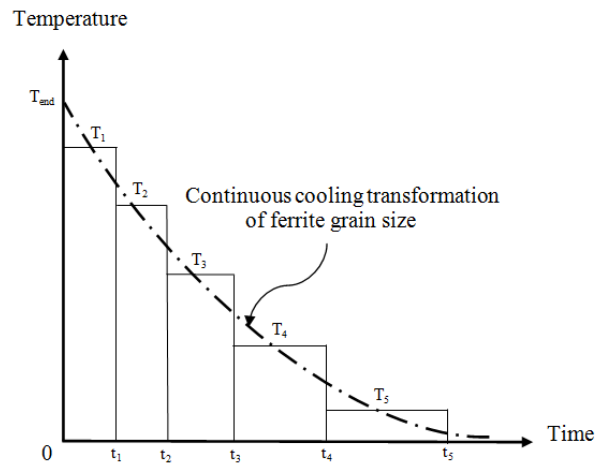


Figure 3. Schematic illustration of continuous cooling transformation in this research material, $T_{1..5}$ as any temperature of transformed cooling curve from T_1 to T_5 , and $t_{1..5}$ as anytime of transformed cooling curve from t_1 to t_5 .

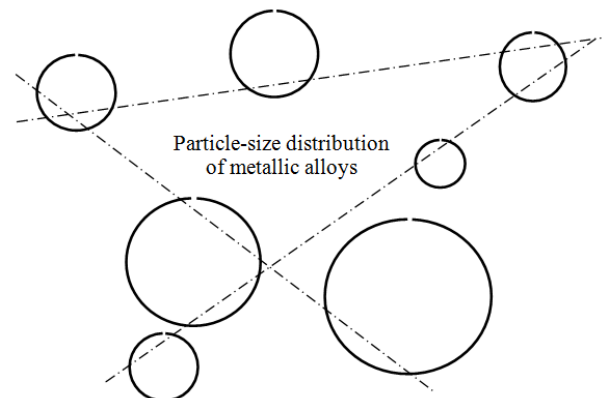


Figure 4. Chords as measurements required for obtaining particle-size distributions, when dealing with relationships between statistical distributions of particles and the properties of alloys.

spheres whose centers lie within a cylinder of unit length and radius x . If there are $N_v(j)$ center of spheres per unit volume of the structure, then the number of chords (ranging in length from l_i to d_j) per unit length of the secant will be

$$N_{L(i,j)} = \pi x^2(i,j)N_{v(j)} = \frac{\pi}{4}(d_j^2 - l_i^2)N_{v(j)} \quad (4)$$

The analysis of the distribution of spherical particles may be simplified if a continuous function is not required. Usually it is sufficient to represent the distribution of particle size as a discontinuous function with a limited number of class intervals. The working formula is obtained (DeHoff & Rhines, 1968).

$$N_{v(i)} = \frac{4}{\pi \Delta^2} \left[\frac{N_{L(i)}}{2i-1} - \frac{N_{L(i+1)}}{2i+1} \right] \quad (5)$$

The mechanical properties of metallic materials have shown to correlate with the microstructural dimensions, most commonly with the average grain size. Based on the work of Hall-Petch, a relationship was found between grain size and the mechanical properties of steel. For yield strength the relationship is formulated (Lehto *et al.*, 2014; Yu, Xin, Wang, & Liu, 2018; Yuan, Panigrahi, Su, & Mishra, 2011):

$$\sigma_y = \sigma_0 + kd^{-1/2} \quad (6)$$

where σ_0 is the lattice friction stress when dislocation move on the slip plane, k is the stress concentration factor or a material-dependent constant known as the Hall-Petch slope, and d is the average grain size. The objective is to study the grain size distribution of a welded micro-alloyed ABS EH36 steel and its influence on the Hall-Petch relationship. Furthermore, methods for the characterization of the grain size distribution are extended to be applicable for that welded steel microstructure.

2. Experimental Procedure

Micro-alloyed ABS EH36 steel in this research is welded by using shielded metal arc welding (SMAW). The welding process is operated on some base metal strip with AWS A5.1 E7016, 2.6 mm (SUMI steel LD-52, low hydrogen potassium, 490 N/mm²-class high strength steel), commercial filler metal. This process of SMAW that can be used to weld many metals, as it depends on the filler arc force that provides deep penetration for the 0.070 %C base metal (Figure 5) (Askeland, 1996; Kalpajian, 1997; SMAW Process, 2019). The set of ten cube specimens from commercial strip to create some prior austenite grain size microstructure and their composition (wt%), (with contents of 0.07C, 0.322Si, 1.483Mn, 0.01P, 0.002S, 0.024Cr, 0.012Mo, 0.056Ni, 0.003V, 0.033Al, 0.077Cu, 0.01Ti, 0.017Nb, Fe) as 10 mm length, with a rectangular cross section 10 mm wide, by 4 mm thick and also the ten butt welded specimens for tensile stress testing were investigated. They are made of the two parts of micro-alloyed ABS EH36 steel as any part as 150 mm wide x 300 mm length x 4 mm thick (Figure 6) (Brnic *et al.*, 2014; Bungmek & Pluphrach, 2016; Buchely, Colorado, & Jaramillo, 2015; Kchaou *et al.*, 2014). The strips set is first pre-

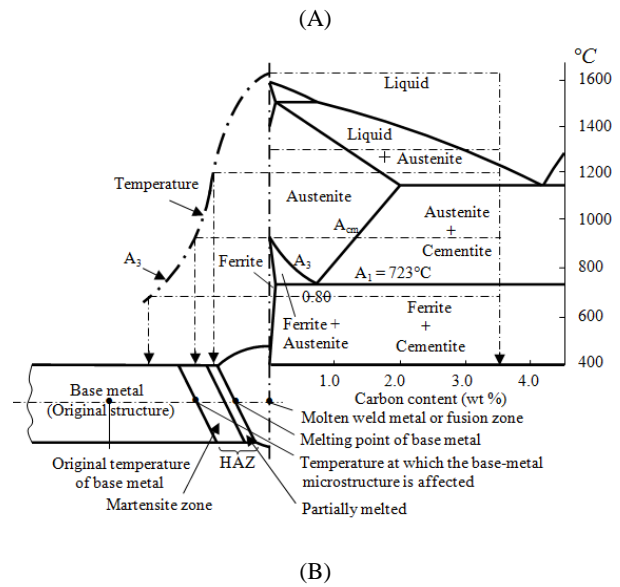


Figure 5. Schematic illustration of (A) various regions in a fusion weld zone by using SMAW process and the corresponding phase diagram for 0.070 percent carbon of a welded micro-alloyed ABS EH36 steel, (B) SMAW filler arc force for some deep penetrated weld.

Ten butt welded specimens for simple-tensile test

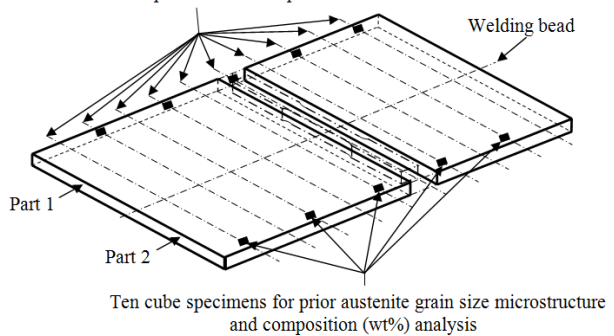


Figure 6. Schematic drawing of the strip showing the specimens extraction of ten cubes and butt welded.

pared by EDM wire cutting for all specimens of the cubes, and butt welded tensile which chamfering and grinding the edges in order to make the 60° V-groove form, respectively (Figure 7) (Ghosh, Kulkarni, Kumar, & Dhiman, 2007; Sundar Singh Sivan *et al.*, 2018). Selected tensile specimens testing for no welded joint base metal (NWJ) and welded joint base metal (WJ) are finished (Figure 7).

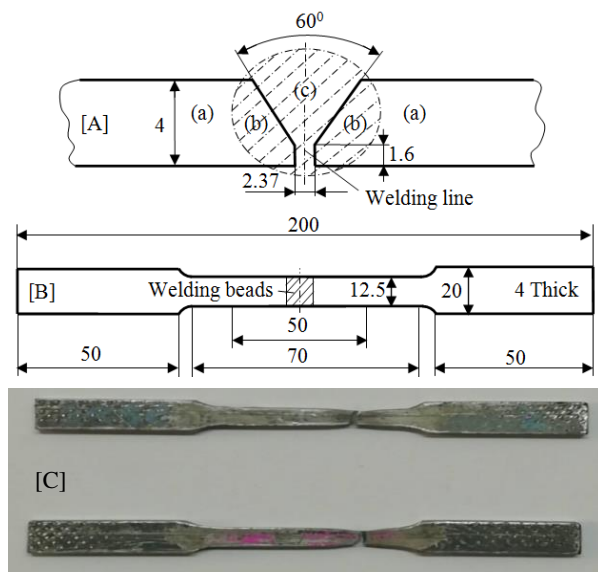


Figure 7. Schematic drawing showing: [A] Scheme of butt welded joint as (a) Base metal, (b) HAZ, (c) Fusion zone, [B] Some machined tensile specimen (testing for NWJ and WJ) that based on the ASTM standard test methods for tension testing of metallic materials, all dimensions are in mm and not to scale, and [C] Selected tensile specimens of NWJ (Top) and WJ (Bottom).

Since prior austenite grain size distribution of micro-alloyed ABS EH36 steel is important factor before the welded operation, and ferrite grain size distribution of the same steel is also important factor after the welded operation, according to the Equation (4). The prior austenite and ferrite grain size microstructures of all the relevant samples representative photomicrographs were revealed. The samples were completely etched in saturated picric acid solution based etchant at about 80°C and in 2% nital solution for evaluated the mean grain size of the prior austenite and ferrite grain boundaries of the specimens, respectively. Determination of grain size in multiphase alloys (Figure 8) (Bungmek & Pluphrach, 2016), requires the measurement of volume fraction and of grain size for each phase separately. The heat-affected zone as multiphase alloys usually includes coarse-grained zone (CGHAZ), fine-grained zone (FGHAZ) and intercritical zone (ICHAZ) (Figure 9). Both determinations can be carried out in one operation with an automatic linear analysis stage (Vander Voort, 2010). It is necessary that intercept sums and the number of intercepts for each phase be recorded in separate counters. The method is of interest for structures of Widmanstätten type and small precipitate. Linear intercept of grains in the micro-alloyed steel, ABS EH36, with polyhedral microstructure is a system of chords with random length along a test line, the derivation by Spektor appears to be the first, as number of intersection points between grain boundaries and a test line (Figure 10) (ISO643, 2003; Vander Voort, 2010).

3. Results and Discussion

Uniaxial tensile tests were performed on selected specimens of NWJ and WJ respectively at room temperature.

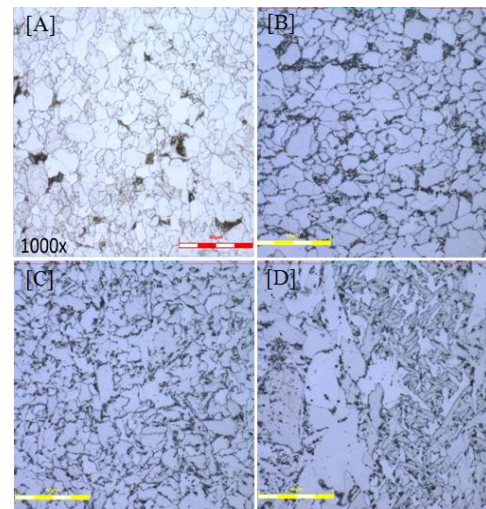


Figure 8. Optical microstructure of the steels in same scale [A] the prior austenite grain size from the selected cube specimens of the micro-alloyed ABS EH36 strip steel, and the same steel from the selected three ferrite-pearlite welded zone of [B], [C], [D] as Base metal, HAZ and Fusion zone, respectively.

Selected tensile curves of the specimens are presented (Figure 11). The tensile properties of NWJ and WJ are concluded, as shown in Table 1. Both NWJ and WJ specimens show a ductile behavior that is in concordance to the specific tensile properties. Certainly, it can be found that yield stress and max stress (ultimate tensile strength) of NWJ specimen are higher than WJ. Meanwhile the elongation of NWJ specimen is also higher than WJ which can be confirmed by the necking coefficient values are as shown in Table 1 as 50% and 58% of striction, respectively. The difference between the yield stress and max stress of NWJ specimen as 452.89 and 525.64 MPa respectively, emphasizes that the ability of this steel to monotonic deformation endured.

The prior austenite grain size of the selected cube specimens of the micro-alloyed ABS EH36 strip steel and the same steel of the selected weld specimens as three ferrite-pearlite welded zone as Base metal, HAZ and Fusion zone are necessary to compare the grains size and yield stress between the difference in multiphase alloys, shown in Table 1 and 2. Referring to the variation of yield stress with $d_a^{-1/2}$, (Figure 12), the following Hall-Petch relationships can be expressed for the ABS EH36 strip steel as (Kazeminezhad & Taheri, 2004)

$$\sigma_y = 35.77 + 0.881d_a^{-1/2} \quad (7)$$

where σ_y and d_a are yield stress and mean ferrite grain size. Hardness measurements, the profiling of microhardness over the welded bead (Figure 7) is already shown (Figure 12). It can be said that, the measured values are not scattering, the maximum hardness value at the middle of fusion zone gets to 192.61 HV, and then it decreases at the base metal to 151.47 HV. The more level of the microhardness in fusion zone can be partially described by the microstructural refinement because of the rapid cooling of the fusion zone (Figure 13).

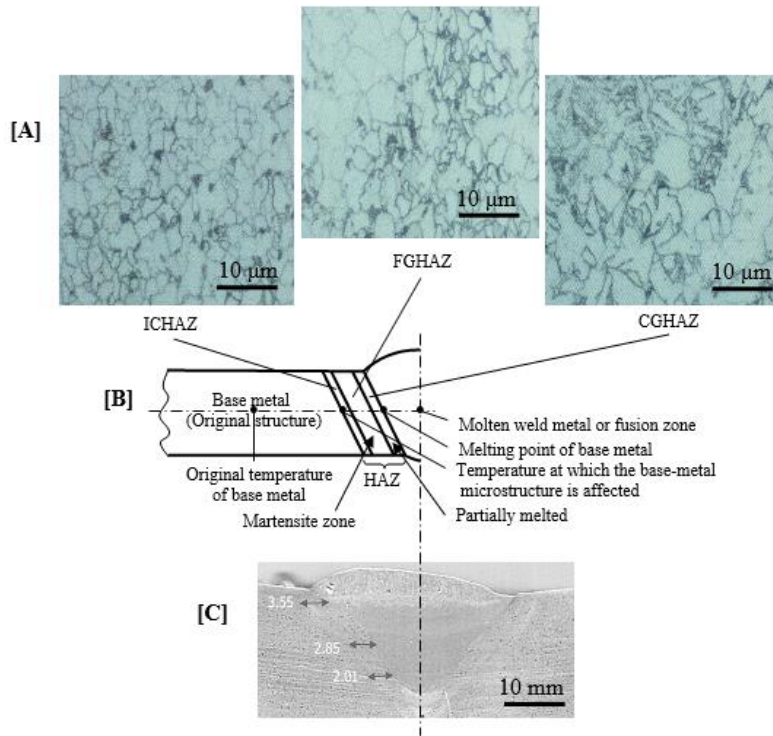


Figure 9. This figure explains that; [A] microstructure of different sub-zones [B] HAZ model showing the three sub-zones of ICHAZ, FGHAZ, and CGHAZ and [C] the welding work that shows the distance of HAZ in mm.

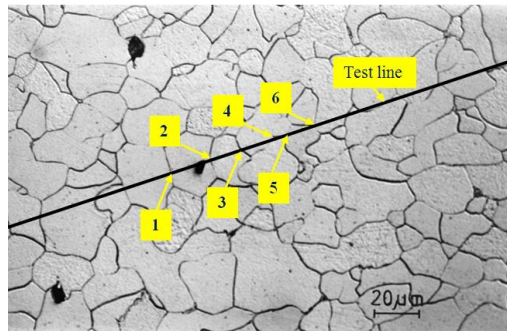


Figure 10. Number of intersection points between grain boundaries and a straight test line placed over a single-phase austenite (or ferrite) microstructure of the same steel, where the arrows show to 6 intersection points as $P = 6$.

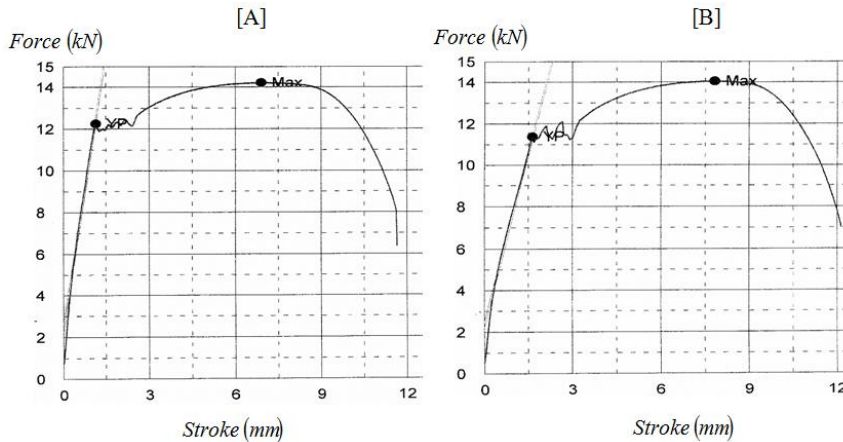


Figure 11. Selected tensile curve of [A] NWJ and [B] WJ at room temperature.

Table 1. Tensile properties of selected specimens of NWJ and WJ.

Types	Yield force (kN)	Yield stress (MPa)	Max force (kN)	Max stress (MPa)	Elongation (%)	Striction (%)
NWJ	12.26	452.89	14.23	525.64	38.21	50
WJ	11.79	416.90	14.45	511.18	35.08	58

Table 2. Size distribution of prior austenite grains of the five selected cube specimens of the micro-alloyed ABS EH36 strip steel.

Items of cube specimens	Range of chord lengths, μm	Number of chords per mm, $N_L(j)$	mm^{-1} , $N_L(j)$	Diameter of grains, mm, d_j	Number of grains per mm^3 , $N_v(j)$	Evaluated mean grain size in true scale, μm , $\bar{d} = \frac{1}{N_v} \sum_{j=1}^m d_j(N_v)_j$
1	0-160	245	19.11	0.016-0.160	1.8899×10^5	5.43
2	0-210	165	15.07	0.021-0.210	0.895×10^5	5.75
3	0-210	217	19.83	0.021-0.210	1.7325×10^5	6.03
4	0-170	231	19.72	0.017-0.170	1.5417×10^5	6.12
5	0-200	238	21.76	0.020-0.200	2.4826×10^5	5.95

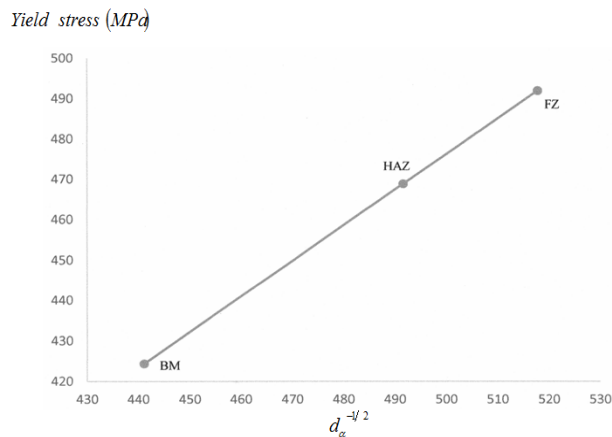


Figure 12. Effect of mean ferrite grain size of three welded zone on yield stress from the selected WJ specimens.

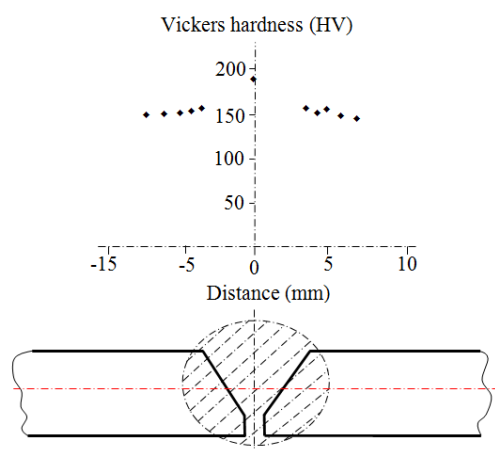


Figure 13. Profiling of microhardness from the scheme of butt welded joint of Figure 7.

4. Conclusions

The investigation conclusions of the influence of prior austenite grain size distribution on the microstructure and mechanical properties of a welded micro-alloyed ABS EH36 steel may be drawn the following from the results presented in this paper:

- 1) The prior austenite grain size distribution, temperatures and time all have significant effects on evolution of the average ferrite grain size and distribution of welded micro-alloyed ABS EH36 steel.
- 2) The prior austenite and ferrite grain boundaries were shown by using various etchants, namely picric acid and nital etching solution, respectively. The composition of two etchants, temperature and etching time were varied for the optimization of etching result along the range of carbon contents. The metallographic results give the principle of grain growth and grain size distribution for some analysis.
- 3) Ferrite grain size, d_α formed by transformation to continuous cooling rate, modeling shown in Fig. 3, at the welding bead zone of micro-alloyed ABS EH36 steel, is decreased with an increase about cooling rate or decrease in welding temperature.
- 4) As alloying is one of the kernel methods to accomplish excellent combination of the significant structure and properties in welded micro-alloyed ABS EH36 steel. During welding, alloying elements are performed to the HAZ phase transformation, because it's equally some process of a heat treatment. A prior study (Ju *et al.*, 2012) showed that the lowest critical crack-tip opening displacement (CTOD) and highest ductile to brittle transition temperature (DBTT) were noticed in CGHAZ because of the undesired microstructure. As a result, the objective of the best microstructure take to increased properties in HAZ, are major addition and optimization of alloying elements in BM, combined with welding methods.
- 5) The Hall-Petch equation can be applied to study the reliance of yield stress on ferrite grain size of this steel studied in the research work.

- 6) The mechanical properties about all of the complete testing, that is to say, yield stress, tensile strength and microhardness, are in good approval and shown that NWJ and WJ, when they show a rupture as in a mode of ductile, the ductility from NWJ is so clear.
- 7) This is a good correlation between experimental and predicted prior austenite and ferrite grain size that determined by Spektor's method and estimated according to ISO standard 643 and yield stress of this steel studied in the research work.

Acknowledgements

The authors would like to express their gratitude to K. Macek, Faculty of Mechanical Engineering, Czech Technical University in Prague, Czech Republic, for his help with some experiments, invaluable discussions, the Strategic Wisdom and Research Institute, Srinakharinwirot University, the Faculty of Engineering, Srinakharinwirot University and the Srinakharinwirot University, Thailand. This research is acknowledged and for the consent to publish this paper.

References

- Adrian, H., & Wiecek, K. (2015). Austenite grain size estimation in structural steel by linear section method. *Archives of Metallurgy and Materials*, 60(4), 2463-2469. doi:10.1515/amm-2015-0400
- Askeland, D. R. (1996). *The science and engineering of materials* (3rd S.I. ed.). Oxford, England: Chapman and Hall.
- Austenite. (2019). Retrieved from <https://en.wikipedia.org/wiki/Austenite>
- Brnic, J., Yurkalj, G., Lanc, D., Canadija, M., Brcic, M., & Vukelic, G. (2014). Comparison of material properties: Steel 20MnCr5 and similar steels. *Journal of Constructional Steel Research*, 95, 81-89. doi:10.1016/j.jcsr.2013.11.024
- Brooks, C. R. (1992). *Principles of the Austenitization of Steels*. Essex, England: Elsevier Science Publishers.
- Buchely, M. F., Colorado, H. A., & Jaramillo, H. E. (2015). Effect of SMAW manufacturing process in high-cycle fatigue of AISI 304 base metal using AISI 308L filler metal. *Journal of Manufacturing Processes*, 20(1), 181-189. doi:10.1016/j.jmapro.2015.08.005
- Bungmek, N., & Pluphrach, G. (2016). Ferrite grain size and mechanical properties in the weld HAZ of a high-strength low-carbon microalloyed steel. *Kasem Bundit Engineering Journal*, 6(2), 1-17. Retrieved from <https://www.tci-thaijo.org/index.php/kbej/issue/view/6878>
- Chen, R. C., Hong, C., Li, J. J., Zheng, Z. Z., & Li, P. C. (2017). Austenite grain growth and grain size distribution in isothermal heat-treatment of 300M steel. *Procedia Engineering*, 207, 663-668. doi:10.1016/j.proeng.2017.10.1038
- Das, S., Ghosh, A., Chatterjee, S., & Ramachandra, R. P. (2003). The effect of cooling rate on structure and properties of a HSLA Forging. *Scripta Materialia*, 48(1), 2463-2469. doi:10.1016/S1359-6462(02)00345-7
- DeHoff, R. T., & Rhines, F. N. (1968). *Quantitative microscopy*. New York, NY: McGraw-Hill Book.
- Ghosh, P. K., Kulkarni, S. G., Kumar, M., & Dhiman, H. K. (2007). Pulsed current GMAW for superior weld quality of austenitic stainless steel sheet. *ISIJ International*, 47(1), 138-145. doi:10.2355/isijinternational.47.138
- International Standard (ISO643). (2003). Steels-Micrographic determination of the apparent grain size (2nd ed.).
- Irshad, M. A. (2011). *The effect of prior austenite grain size on the machinability of a pre-hardened mold steel* (Master thesis, Karlstad University, Karlstad, Sweden). Retrieved from <http://www.diva-portal.se/smash/get/diva2:457589/FULLTEXT01.pdf>
- Ju, J. B., Kim, W. S., & Jang, J. I. (2012). Variations in DBTT and CTOD within weld heat-affected zone of API X65 pipeline steel. *Materials Science and Engineering: A*, 546, 258-262. doi:10.1016/j.msea.2012.03.062
- Kalpakjian, S. (1997). *Manufacturing process for engineering materials* (3rd ed.) Toronto, Canada: Addison-Wesley Longman.
- Kazeminezhad, M., & Taheri, A. K. (2004). Prediction of ferrite grain size and tensile properties of a low carbon steel. *Materials Science and Technology*, 20(1), 106-110. doi:10.1179/174328413X13789824293704
- Kchaou, Y., Haddar, N., Hénaff, G., Pelosin, V., & Elleuch, K. (2014). Microstructure, compositional and mechanical investigation of shielded metal arc welding (SMAW) welded superaustenitic UNS N08028 (Alloy 28) stainless steel. *Materials and Design*, 63, 278-285. doi:10.1016/j.matdes.2014.06.014
- Lehto, P., Remes, H., Saukkonen, T., Hänninen, H., & Romanoff, J. (2014). Influence of grain size distribution on the Hall-Petch relationship of welded structural steel. *Material Science and Engineering A*, 592, 28-39. doi:10.1016/j.msea.2013.10.094
- Pluphrach, G. (2005). Ferrite Grain Size Compared to Austenite Grain Size of Microalloyed Steels in As-Cast State. *Journal of Technology Thonburi*, 4(2), 22-32.
- Pluphrach, G., & Yamsai, S. (2018). Estimation of ferrite grain size and mechanical properties of a 22Mn VNb6 microalloyed low carbon cast steel. *Periodica Polytechnica Mechanical Engineering*, 62(1), 83-89. doi:10.3311/PPme.11458
- Reiter, J., Bernhard, C., & Presslinger, H. (2008). Austenite grain size in the continuous casting process: metallographic methods and evaluation. *Materials Characterization*, 59(6), 737-746. doi:10.1016/j.matchar.2007.06.003
- Show, B. K., Veerababu, R., Balamuralikrishnan, R., & Malakondaiah, G. (2010). Effect of vanadium and titanium modification on the microstructure and mechanical properties of a microalloyed HSLA steel. *Material Science and Engineering A*, 527(6), 1595-1604. doi:10.1016/j.msea.2009.10.049
- SMAW Process. (2019). Retrieved from https://en.wikipedia.org/wiki/Shielded_metal_arc_welding
- Sundar Singh Sivam, S. P., Saravanan, K., Pradeep, N., Moorthy, K. S., & Rajendrakumar, S. (2018). Grey relational analysis and anova to determine the

- optimum process parameters for friction stir welding of Ti and Mg alloys. *Periodica Polytechnica Mechanical Engineering*, 64(4), 277-283. doi:10.3311/PPme.12117
- Vander Voort, G. F. (2010). Revealing prior-austenite grain boundaries. *Microscopy and Microanalysis*, 16 (Suppl. 2), 774-775. doi:10.1017/S1431927610053973
- Wang, X. L., Ma, X. P., Wang, Z. Q., Subramanian, S. V., Xie, Z. J., Shang, C. J., & Li, X. C. (2019) Carbon microalloying effect of base material on variant selection in coarse grained heat affected zone of X80 pipeline steel. *Materials Characterization*, 149, 26-33. doi:10.1016/j.matchar.2019.01.005
- Yu, H., Xin, Y., Wang, M., & Liu, Q. (2018). Hall-Petch relationship in Mg alloys: A review. *Journal of Material Science and Technology*, 34, 248-256. doi:10.1016/j.jmst.2017.07.022
- Yuan, W., Panigrahi, S. K., Su, J. Q., & Mishra, R. S. (2011). Influence of grain size and texture on Hall-Petch relationship for a magnesium alloy. *Scripta Materialia*, 65, 994-997. doi:10.1016/j.scriptamat.2011.08.028